

---

# TFN: AN INTERPRETABLE NEURAL NETWORK WITH TIME-FREQUENCY TRANSFORM EMBEDDED FOR INTELLIGENT FAULT DIAGNOSIS

---

**Qian Chen**

Shanghai Jiao Tong University  
chenqian2020@sjtu.edu.cn

**Xingjian Dong** \*

Shanghai Jiao Tong University  
donxij@sjtu.edu.cn

**Guowei Tu**

Shanghai Jiao Tong University  
guoweitu@sjtu.edu.cn

**Dong Wang**

Shanghai Jiao Tong University  
dongwang4-c@sjtu.edu.cn

**Baoxuan Zhao**

Shanghai Jiao Tong University  
bxzhao@sjtu.edu.cn

**Zhike Peng**

Shanghai Jiao Tong University  
z.peng@sjtu.edu.cn

## ABSTRACT

Convolutional Neural Networks (CNNs) are widely used in fault diagnosis of mechanical systems due to their powerful feature extraction and classification capabilities. However, the CNN is a typical black-box model, and the mechanism of CNN's decision-making are not clear, which limits its application in high-reliability-required fault diagnosis scenarios. To tackle this issue, we propose a novel interpretable neural network termed as Time-Frequency Network (TFN), where the physically meaningful time-frequency transform (TFT) method is embedded into the traditional convolutional layer as an adaptive preprocessing layer. This preprocessing layer named as time-frequency convolutional (TFconv) layer, is constrained by a well-designed kernel function to extract fault-related time-frequency information. It not only improves the diagnostic performance but also reveals the logical foundation of the CNN prediction in the frequency domain. Different TFT methods correspond to different kernel functions of the TFconv layer. In this study, four typical TFT methods are considered to formulate the TFNs and their effectiveness and interpretability are proved through three mechanical fault diagnosis experiments. Experimental results also show that the proposed TFconv layer can be easily generalized to other CNNs with different depths. The code of TFN is available on <https://github.com/ChenQian0618/TFN>.

**Keywords** Convolutional neural network (CNN) · time-frequency transform · TFconv layer · interpretability · fault diagnosis.

## 1 Introduction

Nowadays, fault diagnosis of mechanical equipment is widely used in industry to reduce property damage and improve production efficiency [1, 2]. With the development of sensor technology and industrial internet, a large amount of operation and maintenance data could be obtained by various sensors [3], such as accelerometers, dynamometers, and microphones. With sufficient operation and maintenance data, the data-driven method [4], as a model-free solution with high diagnostic accuracy, has gradually gained more and more attention in the field of mechanical equipment fault diagnosis.

The process of data-driven fault diagnosis can be divided into three steps: data acquisition, feature extraction, and fault classification [5]. Among these steps, feature extraction is the key to fault diagnosis [6, 7]. Traditional feature extraction mainly relies on signal processing methods, including Fourier Transform (FT), Short Time Fourier Transform (STFT), Wavelet Transform (WT) [8] and Empirical Mode Decomposition (EMD) [9]. Using these methods, researchers transform raw maintenance data (i.e., vibration signals) from the time domain into the frequency or time-frequency

---

\*Corresponding Author.

domain, and thus to extract essential features for fault classification. Such a strategy requires much expertise and prior knowledge, which is difficult to obtain in real engineering. Therefore, deep learning, conducting feature extraction and classification automatically, is gaining more and more attention for mechanical fault diagnosis [5].

As a powerful representation learning technique, deep learning provides end-to-end solutions and is widely used in computer vision [10], natural language processing [11], game competition [12] and other fields. In terms of fault diagnosis, deep learning has a series of nonlinear mapping layers to extract hidden key information from vibration signals. Many deep learning models have been applied to mechanical fault diagnosis, such as deep belief network (DBN) [13], convolutional neural network (CNN) [14–16], and recurrent neural network (RNN) [17]. Among these neural networks, CNN-based models can fully extract the spatial information of the input signal and thus leads to high diagnostic accuracy in multiple public datasets for mechanical fault diagnosis [18].

Despite its superior diagnostic performance, the CNN has a weak spot - its interpretability [19]. It is difficult to find the logical foundation of the CNN model for feature extraction and classification. This reduces the credibility of results and prohibits the breakthrough of the model performance, which in turn limits its application in high-reliability-required fault diagnosis scenarios (e.g. aero engine fault diagnosis [20]). Therefore, it is of great importance to develop interpretable CNNs for high-quality fault diagnosis of mechanical systems.

The research of interpretable CNN is a growing research field [21, 22]. Current interpreting methods can be roughly divided into four categories [23]: rule type, semantic type, attribution type, and example type. Rule type is to extract the mapping relationship of CNNs into specific logical rules (e.g. CEM [24], CDRP [25]). Semantic type is to completely analyze the meaning of specific hidden layers in CNNs (e.g. Network dissection [26]). Attribution type is to quantify the contribution (or negative effect) of the input and features (e.g. salient map [27], Grad-CAM [28], IG [29]). Example type is to summarize typical samples related to the category (e.g. Influence functions [30]). The above interpreting methods are mainly designed for 2D images. When it comes to 1D vibration signals in mechanical fault diagnosis, these techniques are not suitable.

At present, there are few studies to explore the interpretability of CNNs in the field of mechanical fault diagnosis. Li *et al.* [31] calculated the importance weight of each point of the vibration signal sample to the CNN prediction through the integrated gradient (IG) method, and they explained the foundation of prediction-making through the frequency spectra of calculated weights. Wu *et al.* [32] transformed 1D vibration signals into 2D time-frequency spectra as the input samples, such that 2D interpreting method (i.e. Grad-CAM) could be adopted to obtain the model attention area. Wang *et al.* [33] extended the extreme learning machine (ELM) to an interpretable structure for machine state monitoring. With this strategy, the information frequency band can be automatically located. Zhao *et al.* [34] incorporated the Reproducing Kernel Hilbert Space (RKHS) into the convolutional layer and built a specific interpretable denoising convolutional layer. Li *et al.* [35] combined continuous wavelet transform with convolutional layers to formulate a wavelet kernel network to extract interpretable features. The above studies help to explain the mechanism of CNNs in fault diagnosis to some extent, but their interpretations are usually ambiguous and need subjective understandings (e.g. the similarity between different frequency spectra of inputs [31], the sensibility of CNN to impulsive signal [35]). On top of that, these strategies brought some other issues: the degraded diagnostic performance and the poor generalizability.

To proposed an interpretable CNN model for fault diagnosis, we set our sights on signal processing methods which is physically meaningful and good at feature extraction. Considering that the Fourier-type transform and the convolution can be both regarded as inner products, we embedded the time-frequency transform (TFT) method into the traditional convolutional layer. This leads to a novel layer named time-frequency convolutional (TFconv) layer, which is constrained by a well-designed kernel function in order to extract fault-related time-frequency information. Using the TFconv layer as preprocessing layer, we constructed the Time-Frequency Network (TFN) for fault diagnosis tasks. With the interpretable TFN, we revealed the logical foundation of prediction-making in the frequency domain through the frequency response analysis. A series of mechanical fault diagnosis experiments verify the superior diagnostic performance and the clear interpretability of TFN. The main contributions of this study could be summarized as follows.

1. TFconv layer with excellent interpretability is proposed, with which we can extract time-frequency information to obtain better categorical representations.
2. All the inner product based TFT methods can be embedded into TFconv layer as kernel functions, and four typical TFT methods are considered to formulate corresponding TFconv layers and further be analyzed.
3. TFN is proposed by combining the interpretable TFconv layer with a backbone CNN, and we give the entire procedure of using the TFN in mechanical fault diagnosis.
4. Frequency response analysis is performed on the well-trained TFconv layer to explain the logical foundation of feature extraction and prediction-making of TFN in the frequency domain.
5. TFconv layer can be easily generalized to other CNN models with different depths to improve their diagnostic performances.

The rest of this article is organized as follows. Section II introduces TFT and CNN as the theoretical foundation. Based on Section II, the construction of the TFconv layer, the interpreting method, and the diagnosis procedure by using TFN are presented in Section III. In Section IV, three mechanical dataset tests are carried out to verify the performance of TFN. Section V gives the ablation study, interpretability analysis, visualization analysis, and generalizability analysis of TFN. Finally, Conclusions are given in Section VI.

## 2 Theoretical Foundation

### 2.1 Time-Frequency Transform

Time-frequency transform (TFT) is widely used in signal processing and it is based on inner product. Mathematically, the purpose of inner product is to measure the similarity, and any vector could be decomposed into a set of orthogonal bases by means of inner product. Considering the 1D vibration signal as a vector, we can decompose the signal in the same way. Fourier transform, the most fundamental signal processing method, takes the frequency-orthogonal sine function as the basis and decomposes the vibration signal through inner product to obtain the amplitude of the vibration signal at different frequencies, i.e., the frequency spectrum:

$$X(f) = \int_{-\infty}^{+\infty} x(t)(e^{j2\pi ft})^* dt = \langle x(t), e^{j2\pi ft} \rangle \quad (1)$$

where  $X(f)$  denotes the frequency spectrum,  $x(t)$  denotes the analysed signal,  $e^{j2\pi ft}$  denotes the trigonometric bases and  $*$  denotes the conjugate operator.

Although the frequency spectrum obtained by inner product with frequency-orthogonal bases can effectively reveal the frequency domain information of the vibration signal, it leaves out the time domain information and thus is not suitable for non-stationary signals. To process non-stationary signals, it is necessary to obtain the amplitude of the signal at different times and different frequencies, i.e., the time-frequency spectrum.

The time-frequency spectrum can be obtained by the inner product with time-frequency-orthogonal bases, which is formulated as

$$TF(\tau, f) = \int_{-\infty}^{+\infty} x(t)\psi_f^*(t-\tau)dt = \langle x(t), \psi_f(t-\tau) \rangle \quad (2)$$

where  $TF(\tau, f)$  denotes the time-frequency spectrum,  $X(t)$  denotes the analysed signal,  $\langle \psi_f(t-\tau) \rangle_{f,t}$  denotes the time-frequency-orthogonal bases.  $\psi_f(t)$  denotes the inner product window function that has compact support.

The process of inner product based TFT is demonstrated in Fig. 1. The input signal  $x(t)$  and the inner product window functions  $\psi_f(t)$  with different frequency bands are convolved to obtain the frequency spectrum of the signal at a specific time point  $\tau$ . With the movement of the time point  $\tau$ , the complete time-frequency spectrum  $TF(\tau, f)$  is gradually obtained. Among the process, parameter  $\tau$  and  $f$  are used to adjust the focusing area of inner product window function in time domain and frequency domain respectively. It should be noted that the inner product window function is a complex function, so the obtained time-frequency spectrum is also complex, that is, the spectrum includes both the amplitude information and the phase information. In order to separate the amplitude information, the absolute operation of the time-frequency spectrum is required.

TFT methods include short-time Fourier transform (STFT), Chirplet Transform (CT) [36], and wavelet transform (WT), etc. All these methods follow the above procedure and the only difference is in the inner product window function. STFT constructs an inner product window function by multiplying the sine function by a time domain window. CT introduces a linear frequency modulation factor to STFT, thereby improving the algorithm accuracy and stability for signals under variable speed conditions. WT uses the wavelet family, which is generated by the mother wavelet through scaling and translation, as the inner product window function, so as to obtain a time-frequency window that varies with frequency. WT has low time domain resolution and high frequency domain resolution at the low frequency, and vice versa at the high frequency. Morlet wavelet [37] and Laplace wavelet [38] are two typical wavelets used in wavelet transform. Morlet wavelet is symmetric in time domain and suitable for extracting stationary fault features, while Laplace wavelet is asymmetric and suitable for extracting impulsive fault features. The inner product window functions of the above four TFT methods are shown in Table 1.

TFT methods can project the non-stationary signals from time domain into time-frequency domain to obtain their time-frequency joint information. As shown in Fig. 1, the input signal is simulated for rolling bearing with inner fault, and its time-frequency spectrum demonstrates both the vibration frequency and the dual-impulse property. Due to their powerful analytical abilities, TFT methods play an important role in the feature extraction of mechanical fault diagnosis.

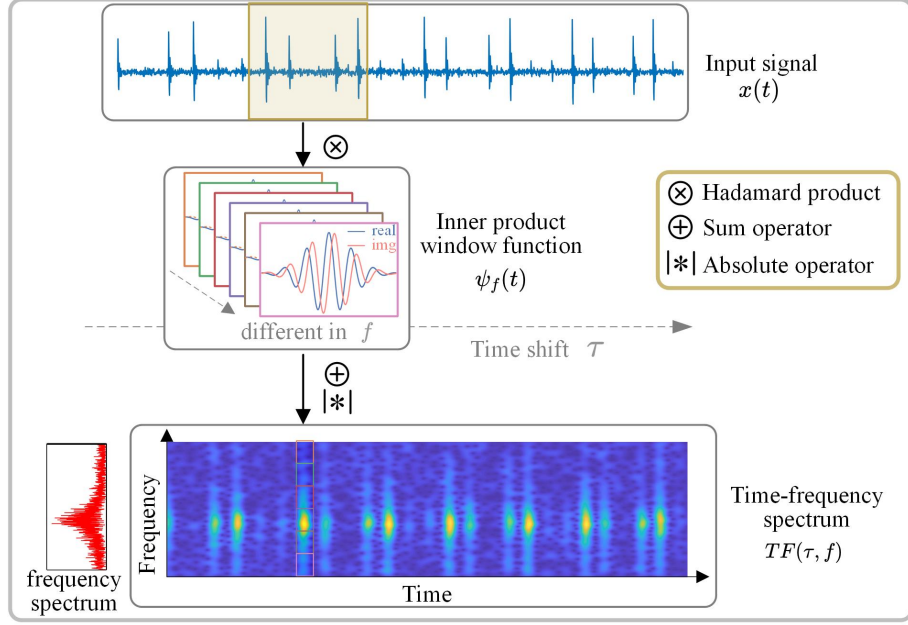


Figure 1: The process of inner product based TFT.

## 2.2 CNN

The structure of convolutional neural network (CNN) can be roughly divided into two parts: convolutional part and classification part. The convolutional part consists a series of convolutional layers, BN layers, activation layers, and pooling layers, while the classification part consists of several fully connected layers. The input samples usually are 1D vibration signals, so the CNN models used for mechanical system fault diagnosis is 1D accordingly.

The convolutional layer is the core part of the CNN and the process of convolution is shown in Fig. 2. Each randomly initialized convolution kernel is convolved along the 1D input signal, and the results of multiple convolution kernels are concatenated to obtain the feature map. The feature map of the  $l$ -th layer on the  $k$ -th channel can be expressed as

$$h_k^l = w_k^l * x^l + b_k^l \quad (3)$$

where,  $x^l$  denotes the input of the  $l$ -th convolutional layer, and  $w_k^l$  and  $b_k^l$  denote the weight and bias of the  $k$ -th convolution kernel in the  $l$ -th convolutional layer respectively. The symbol  $*$  denotes the convolution operator.

The BN layer normalizes inputs to a specific distribution, thereby increasing the training speed and alleviating gradient explosion or disappearance. The output value of the  $k$ -th channel in the  $l$ -th BN layer can be given as

$$\hat{h}_k^l = \frac{h_k^l - \mu_k^l}{\sqrt{\sigma_k^l} + \varepsilon} \quad (4)$$

where  $\mu_k^l$  and  $\sigma_k^l$  denote the channel-wise mean and variance of the input  $h_k^l$ , and  $\varepsilon$  denotes a small constant that prevents the denominator from being zero.

The activation layer introduces nonlinearity into CNN, thereby enabling nonlinear mapping. The output of the  $l$ -th activation layer can be denoted as

$$z^l = f(\hat{h}^l) \quad (5)$$

where  $\hat{h}^l$  denotes the input of the activation layer and  $f$  denotes the nonlinear activation function, e.g. ReLU, sigmoid.

With quite many features extracted, the pooling layer aims to compress them to reduce the model parameters while preserve the main information. The output of the  $l$ -th pooling layer can be denoted as

$$y^l = \text{down}(z^l) \quad (6)$$

where  $y^l$  denotes the input and down denotes downsampling operation, such as maximum or average downsampling.

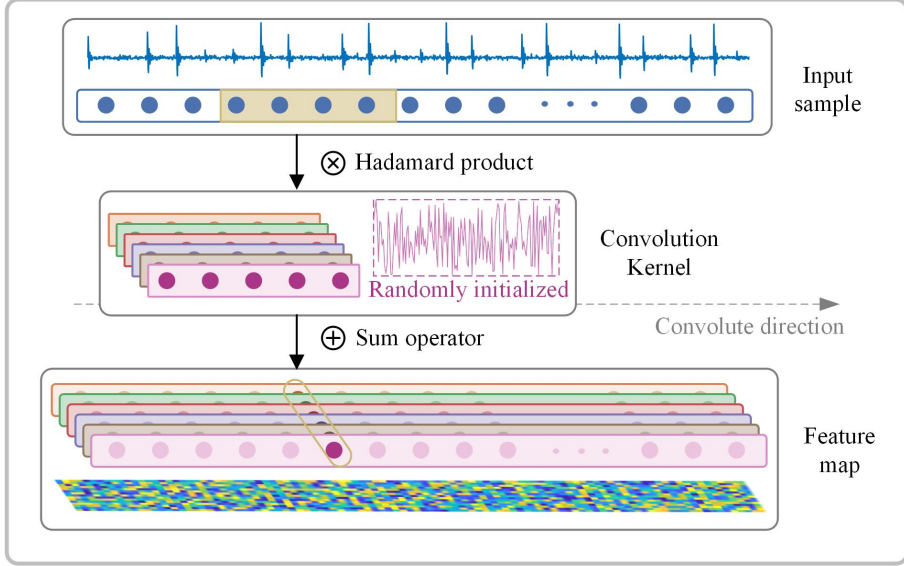


Figure 2: The process of traditional convolutional layer in CNN.

After convolutional part, the raw signal has been transformed into high-dimensional features, which are flattened and further classified in the following classification part. Finally, *Softmax* function is used to obtain the probability of different categories, and classification loss is calculated through cross entropy, which can be given as

$$L(r, p) = - \sum_i r_i \log p_i \quad (7)$$

where  $i$  denotes the number of categories,  $r$  and  $p$  denotes the the ground truth and predicted probability, respectively. The classification loss measures the discrepancy between the true label and the prediction. With the training strategy based on backpropagation (BP) and stochastic gradient descent (SGD) algorithm, the model's prediction can approach to the true label gradually.

### 3 Methodology

In this section, we introduce the structure and the kernel function of TFconv layer, then present its interpreting method, and propose the TFN with the fault diagnosis procedure based on the TFN.

#### 3.1 Structure of TFconv Layer

The TFT method is physically interpretable, but it cannot extract adaptive time-frequency information based on the characteristics of the diagnostic dataset. On the other hand, CNNs can automatically extract high-dimensional features from the original samples and make accurate classifications efficiently, but the mechanism and principle of CNN's decision-making are not clear enough. To utilize the advantages of both two strategies, we embed TFT method into traditional convolutional layer since they can be both regarded as inner products. This leads to a novel layer named the TFconv layer.

We designed the TFconv layer to mimic the physically interpretable TFT method. As demonstrated in Fig. 3, the TFconv layer consists of a real part kernel and an imaginary part kernel, which convolve with the input samples along the length direction to get the real feature and imaginary feature, respectively. After that, the absolute values of real and imaginary features are calculated (as TFT) to obtain the final feature map as the output of TFconv layer, and each channel is processed independently in the whole process. Moreover, different from the traditional convolutional layers whose weights are randomly initialized, the weights of the real and imaginary part kernels correspond to the real and imaginary parts of the kernel function respectively. The control parameter  $\theta$ , which adjusts the frequency property of

kernel function, is treated as trainable parameter and updated in the BP process. The kernel function here is a variant of the inner product window function in TFT, and the output of the  $k$ -th channel of the TFconv layer can be denoted as

$$\begin{cases} h_{k, \text{real}} = \psi_{\theta, \text{real}}^k * x \\ h_{k, \text{img}} = \psi_{\theta, \text{img}}^k * x \\ h_k = \sqrt{h_{k, \text{real}}^2 + h_{k, \text{img}}^2} \end{cases} \quad (8)$$

where  $k$  denotes the number of channels,  $x$  denotes the input of the TFconv layer,  $\psi_{\theta, \text{real}}$  and  $\psi_{\theta, \text{img}}$  denote the real and imaginary part of the kernel function respectively,  $h_{\text{real}}$  and  $h_{\text{img}}$  denote the real and imaginary feature map respectively, and  $h$  denotes the final feature map.

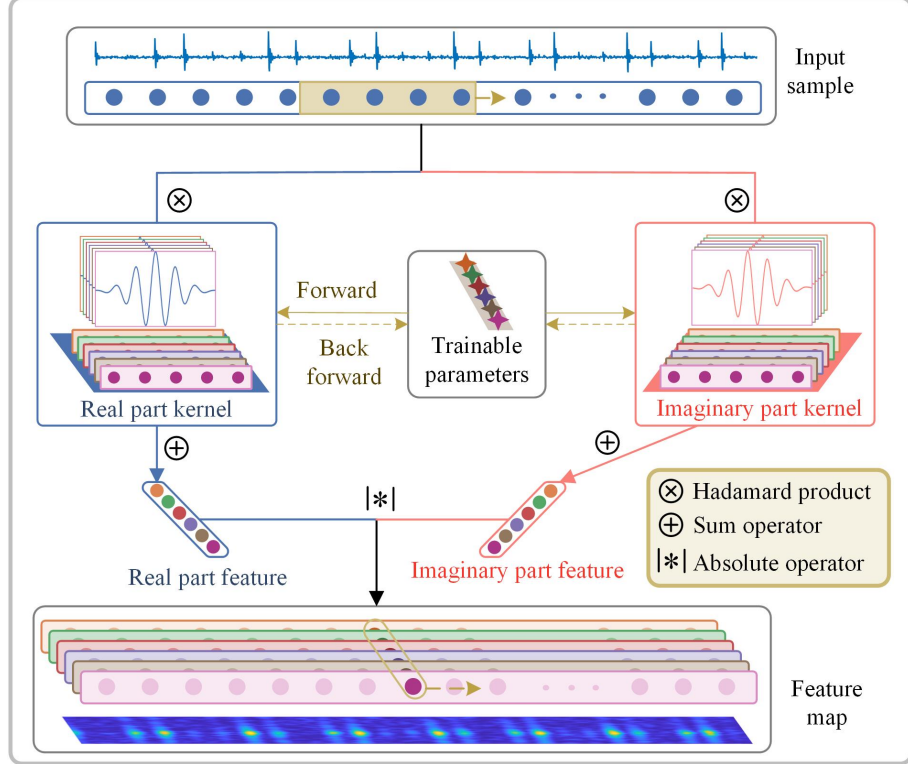


Figure 3: The process of TFconv layer.

As a result, compared to traditional convolutional layers, the proposed TFconv layer has three novel aspects as follows.

1. Real-Imaginary Mechanism: TFconv layer has two convolution processes of the real part and imaginary part, and their outputs are merged through absolute operation.
2. Kernel Function: The weight of the convolution kernel of TFconv layer is determined by the specific kernel function, not randomly initialized.
3. Trainable Parameters: The trainable parameters of TFconv layer are the control parameters  $\theta$  of the kernel function (e.g. frequency factor  $f$  in STFT kernel), instead of the convolutional weights.

Since the trainable parameters of TFconv layer are different from those of the traditional convolutional layer, the BP process of TFconv layer is different accordingly. In the BP process, TFconv layer calculates the gradient of trainable parameters and updates them during each training step, which can be expressed as

$$\begin{cases} \delta_{\theta} = \frac{\partial L}{\partial h} \left( \frac{\partial h}{\partial \psi_{p, \text{real}}} \frac{\partial \psi_{p, \text{real}}}{\partial \theta} + \frac{\partial h}{\partial \psi_{p, \text{img}}} \frac{\partial \psi_{p, \text{img}}}{\partial \theta} \right) \\ \theta \leftarrow \theta - \eta \delta_{\theta} \end{cases} \quad (9)$$

where  $\theta$  denotes the trainable parameters,  $\delta_{\theta}$  denotes the gradient of  $\theta$ ,  $\partial$  denotes the partial derivative operator,  $L$  denotes the classification loss,  $h$  denotes the output of the TFconv layer,  $\psi_{p, \text{real}}$  and  $\psi_{p, \text{img}}$  denote the real and

imaginary part kernels. After the gradient is obtained by the chain rule, the trainable parameters are updated by subtracting the product of the learning rate  $\eta$  and the gradient  $\delta_\theta$ .

### 3.2 Kernel Function of TFconv Layer

The kernel function of TFconv layer derives from the inner product window function of TFT through necessary discretization and modification, which is the key step to embed TFT method into the TFconv layer. With TFT method embedded, physical constraints of TFT are also introduced in TFconv layer, that is, there is a certain limit on the trainable parameters of the kernel function. Taking STFT as an example, due to the *nyquist* sampling theorem, the meaningful normalized frequency is  $[0, 0.5]$ , so the frequency factor  $f$  of the corresponding kernel function should be limited to  $[0, 0.5]$  as well.

According to the above analysis, four typical TFT methods (i.e. STFT, CT, Morlet WT and Laplace WT) are considered to formulate TFconv kernel functions. The inner product window functions of TFT, the corresponding kernel functions of TFconv layer and trainable parameters with their limits are shown in Table 1. Compared with short-time trigonometric function (STTF) and Chirplet function, Morlet wavelet and Laplace wavelet can stretch and contract in time domain by scale factor  $s$ . When they stretch too long, the time-domain truncation may occurs due to limited kernel length, leading to the spectral leakage phenomenon in the frequency domain. Therefore, to avoid time-domain truncation, the kernel length of Morlet wavelet and Laplace wavelet kernel function is designed to be much longer than that of STTF and Chirplet.

Table 1: The Inner Product Functions of Time-Frequency Transform, The corresponding Kernel Functions of TFconv layer and Trainable Parameter with Their Limits

Kernel Function Name	Inner Product Function of Time-Frequency Transform	Kernel Function of TFconv layer	Trainable Parameter with its Limit
STTF	$\psi_{\omega,\sigma}(t) = \frac{1}{\sqrt{2\pi}\sigma} e^{-\frac{1}{2}(\frac{t}{\sigma})^2} \cdot e^{-j\omega t}$	$\psi_f[n] = e^{-\frac{1}{2}(\frac{n}{10})^2} e^{j2\pi f n}$ $n = [-25, -24, \dots, 25]$	$f_0 \in [0, 0.5)$
Chirplet	$\psi_{\omega,\alpha,\sigma}(t) = \frac{1}{\sqrt{2\pi}\sigma} e^{-\frac{1}{2}(\frac{t}{\sigma})^2} e^{-j[\frac{\alpha}{2}t^2 + \omega t]}$	$\psi_{f,\alpha}[n] = e^{-\frac{1}{2}(\frac{n}{10})^2} e^{-j2\pi[\frac{\alpha}{2}t^2 + ft]},$ $n = [-25, -24, \dots, 25]$	$f \in [0, 0.5),$ $\alpha \in (+0.005, -0.005)$
Morlet Wavelet	$\psi_s(t) = \frac{1}{\sqrt{s}} \Psi\left(\frac{t}{s}\right),$ $\Psi(t) = Ae^{-\beta \frac{t^2}{2}} e^{j\omega t}$	$\psi_s[n] = \frac{1}{\sqrt{s}} \Psi\left(\frac{n}{s}\right),$ $\Psi(n) = e^{-\frac{1}{2}(\frac{n}{10})^2} e^{j2\pi \cdot 0.2 \cdot n},$ $n = [-150, -149, \dots, 150]$	$s \in [0.4, 10]$
Laplace Wavelet	$\psi_s(t) = \frac{1}{\sqrt{s}} \Psi\left(\frac{t}{s}\right),$ $\Psi(t) = Ae^{-\frac{\zeta}{\sqrt{1-\zeta^2}\omega t}} e^{j\omega t}$	$\psi_s[n] = \frac{1}{\sqrt{s}} \Psi\left(\frac{n}{s}\right),$ $\Psi(n) = e^{-\frac{1}{2}(\frac{n}{10})^2} e^{j2\pi \cdot 0.2 \cdot n},$ $n = [0, 1, \dots, 150]$	$s \in [0.4, 10]$

To illustrate the properties of above four kernel functions, the time-domain and frequency-domain diagrams of them are shown in Fig. 4. STTF kernel function has a uniform spectral bandwidth, and the center frequency is adjusted by the frequency factor  $f$ . The Chirplet kernel function introduces a linear frequency modulation factor  $\alpha$  to the STTF kernel function to dynamically change the bandwidth. Morlet Wavelet and Laplace Wavelet kernel functions are relatively special. They scale their mother wavelet by scaling factor  $s$  to adjust their frequency properties, and with the increase of scaling factor, they have higher center frequency and wider bandwidth.

As for the initialization of TFconv layer, the channels in TFconv layer are initialized with different control parameters to obtain different focusing frequency area respectively, and these focusing frequency areas are subjected to an uniform distribution overall. This is the exact way of TFT methods working, and the focusing frequency area of an initialized TFconv layer with STTF kernel can be referred to Fig. 5 (b).

### 3.3 Interpretability of TFconv Layer

With TFT method embedded, TFconv layer not only can extract time-frequency information from input samples, but also become explainable through the interpreting method proposed in this subsection. The interpreting method is to perform the frequency response analysis on the trained TFconv layer to obtain its frequency response (FR), which indicates the attention CNN paid to different frequencies. The frequencies of great interest are deeply involved in the prediction-making process and responsible for the results of CNN. The motivation here is consistent with that of the attribution type [23] interpreting methods, but our method is unique in the following two aspects.

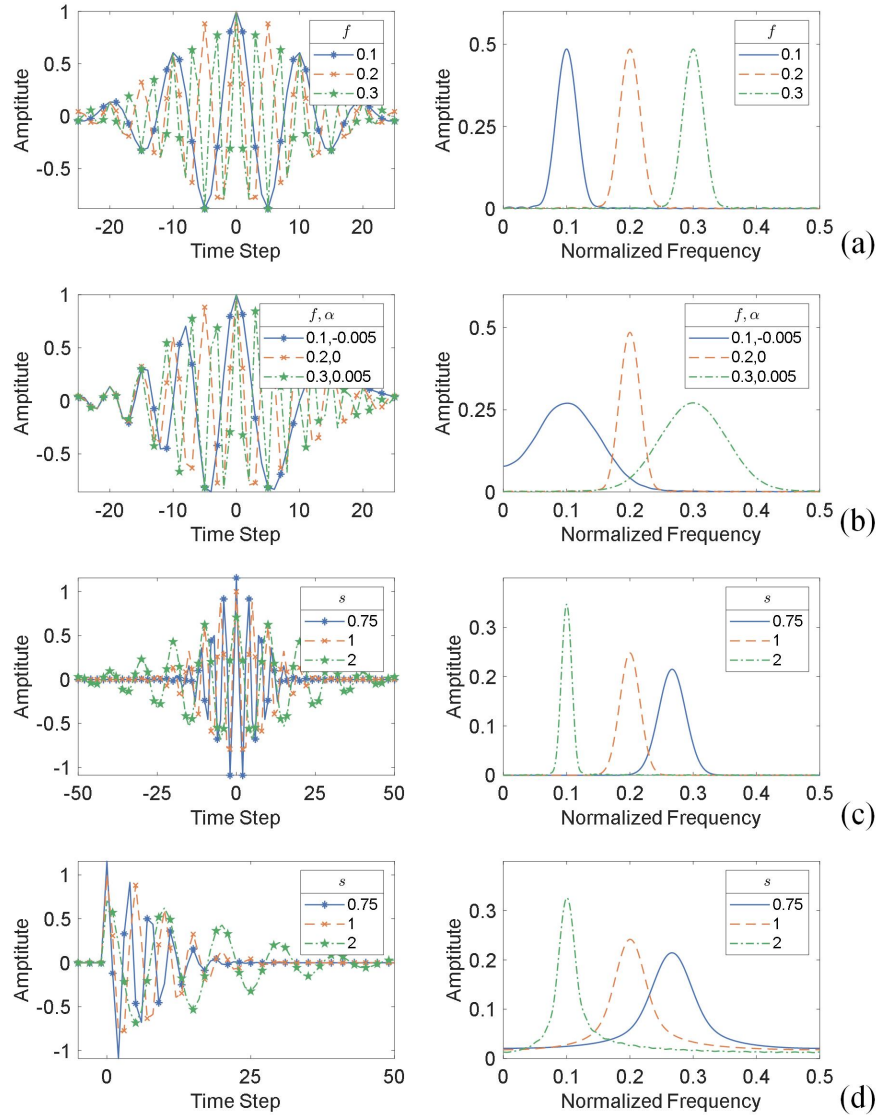


Figure 4: The time-domain and frequency-domain diagrams of four kernel functions of TFconv layer. (a) STTF. (b) Chirplet. (c) Morlet Wavelet. (d) Laplace Wavelet.

1. The attribution of most attribution type methods is the inputs or the features, while that of our interpreting method is the frequency of inputs, which is far more suitable for mechanical fault diagnosis tasks since the frequency is usually correlated with a specific type of machine fault.
2. Most attribution type methods explain the model from a local perspective, that is, they focus on the explanations of one individual prediction. While our method interprets the CNN model in a global perspective that reveals the logical foundation in frequency domain over the entire dataset.

The frequency response analysis of the convolutional layer derives from the filter theory in signal processing area. The convolution process by the convolutional layer is exactly equivalent to the filtering process of finite impulse response (FIR) filter [39]. The convolution kernel can be regarded as the FIR filter, and the input sample is the signal to be filtered. As for the frequency response analysis, the convolution kernel is zero-padded with an appropriate length and then the FFT operation is performed to obtain the FR of the convolutional layer [40]. Considering multiple channels contained in the convolutional layer, we calculate the channel-wise frequency response (C-FR) firstly, and average them to obtain the overall amplitude frequency response (O-FR). The calculation process could be denoted as

$$\begin{aligned} H_i(f) &= \text{FFT}(P(w_i)) \\ H(f) &= \frac{1}{n} \sum_i^n H_i(f) \end{aligned} \quad (10)$$

where,  $w_i$  denotes the convolution kernel of the  $i$ th channel,  $P$  denotes the zero padding operator,  $H_i(f)$  and  $H(f)$  denote the C-FR of  $i$ th channel and the O-FR, respectively. Although the above frequency response analysis is based on the traditional convolutional layer, it is also applicable to the TFconv layer because the weights of real part kernel and imaginary part kernel are derived from the same kernel function.

Both the traditional convolutional layer and the TFconv layer can be conducted by frequency response analysis, yet there still exist some differences in their results. The C-FR and O-FR of traditional convolutional layer and TFconv layer with STFT kernel are shown in Fig. 5. The C-FR of the traditional convolutional layer, shown in Fig. 5 (a), exhibits a random and uniform distribution, which is difficult to identify the focusing frequency area. While the TFconv layer, shown in Fig. 5 (b), is controlled by the kernel function and has a clear frequency preference, where the focusing frequency area can be identified and used for interpreting.

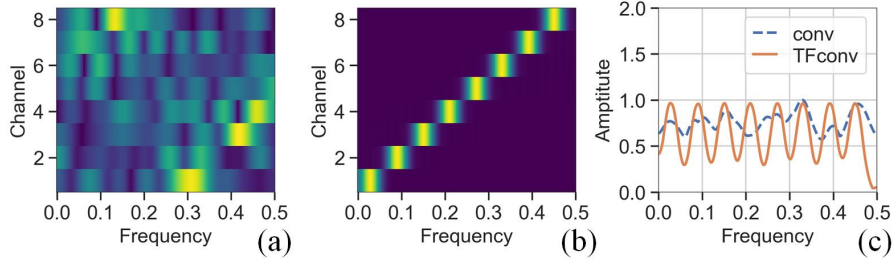


Figure 5: The comparison between C-FR and O-FR of initialized traditional convolutional layer and that of initialized TFconv layer. (a) C-FR of traditional convolutional layer. (b) C-FR of TFconv layer with STFT kernel. (c) O-FR of traditional convolutional layer (denoted as conv) and TFconv layer with STFT kernel.

### 3.4 Fault Diagnosis Using TFN

The interpretable TFconv layer is used as a preprocessing layer to combine with a bonebone CNN, and the resulting novel network is named the Time-Frequency Network (TFN). With TFN, we can extract fault-related time-frequency information from raw vibration signals and diagnose the fault states of mechanical equipment efficiently. The entire process of applying TFN to intelligent mechanical fault diagnosis is summarized as Fig. 6.

First, the vibration signals are collected by the accelerometers installed on the mechanical equipment. Second, the vibration signal is truncated with a sliding window to generate a series of samples as the input of TFN. Third, the kernel function is formulated by TFT method and embedded into TFconv layer. Then, an existing CNN model is selected as the backbone, and the TFconv layer is combined as the preprocessing layer with the backbone to obtain TFN. After that, the obtained TFN is trained and verified by training samples and testing samples in fault diagnosis tasks. Finally, the interpreting method is conducted to reveal the focusing frequency area of TFN.

The algorithm about applying TFN to mechanical fault diagnosis is summarized in Algorithm 1.

---

**Algorithm 1** Applying TFN to Mechanical Fault Diagnosis

---

1 **Data acquisition:** Obtain the training dataset  $X_{\text{train}}$  and the test dataset  $X_{\text{test}}$ .

2 **Model preparation:**

- 1) Design kernel function  $\psi[n]$  according to Table 1;
- 2) Formulate TFconv layer by embedding the designed kernel function  $\psi[n]$ ;
- 3) Select a CNN as the backbone;
- 4) Combine TFconv layer as the preprocessing layer with the backbone CNN.

3 **Model training and validation:**

- 1) Train TFN with dataset  $X_{\text{train}}$ ;
- 2) Update TFconv layer with Equations (9), and update other layer with BP algorithm;
- 3) Validate TFN with dataset  $X_{\text{test}}$ .

4 **Model interpretability:** calculate the focusing frequency area of TFN with Equations (10).

---

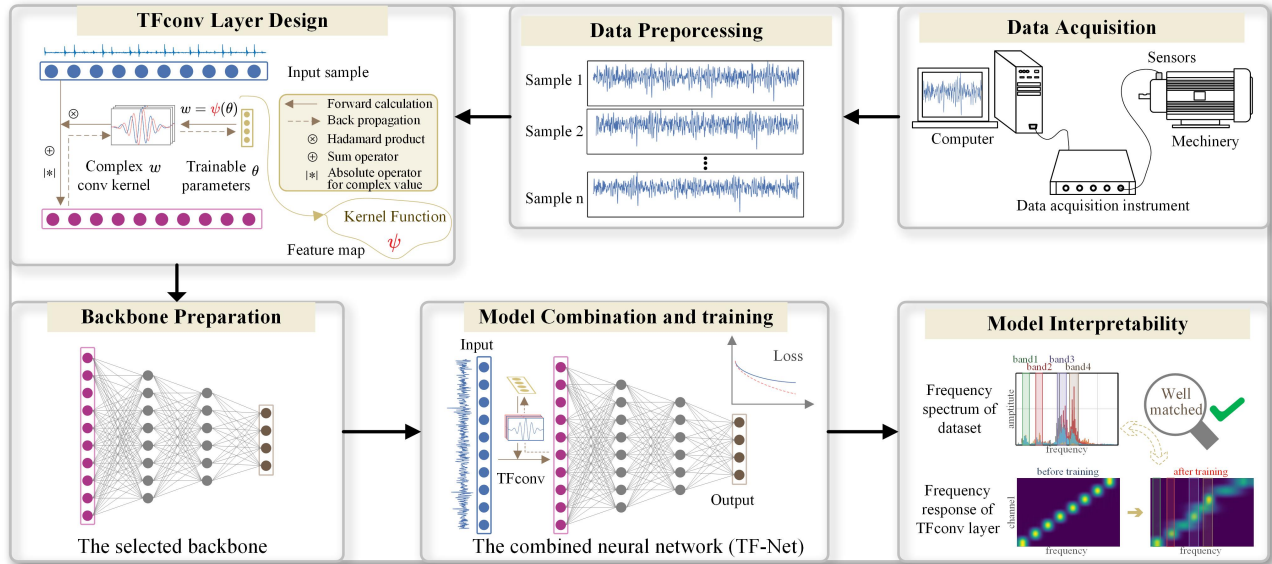


Figure 6: The entire process of applying TFN to intelligent mechanical fault diagnosis

In order to verify the effectiveness of the TFconv layer, a relatively shallow CNN is selected as the backbone, and the architecture of the obtained TFN is shown in Table 2, where  $n_m$ ,  $N$  and  $n_p$  are the channel number, length of the TFconv layer, and the number of categories for classification, respectively.  $n_m$  and  $N$  are determined in the design process of TFconv layer, and  $n_p$  is determined by the specific dataset.

## 4 Experiment

In this section, three experimental datasets are used to verify the effectiveness of TFN and analyze its properties. For comparison, we apply the TFNs with different kernels, the backbone CNN alone, and the TFN with random kernels (i.e. randomly initialized weight and updated by BP algorithm).

### 4.1 Planetary Gearbox Dataset

In this subsection, the performance of TFN is verified by a planetary gearbox system shown in Fig. 7. This planetary gearbox system includes an electric motor, a transmission shaft, a torque transmission, a planetary gearbox, a magnetic powder brake and a series of sensors. The vibration signals are collected by the accelerometer located at the shell of the planetary gearbox and transmitted to the signal acquisition card at the sampling frequency of 10.2 kHz.

Four types of component failures are considered in this experiment, including tooth fractures of three different gears and the outer race pitting of the rolling bearing as shown in Fig. 8. Based on these faults, the experiments are conducted

Table 2: The Architecture of The Analyzed TFN

Part	No. Unit	Basic Unit	Output Size
TFconv	-	input	1*1024
	1	TFconv( $n_m$ @N*1)	$n_m$ *1024
Backbone	2	Conv(16@15*1)-BN-ReLU	16*1010
	3	Conv(32@3*1)-BN-ReLU-MaxPool(2)	32*504
	4	Conv(64@3*1)-BN-ReLU	32*502
	5	Conv(128@3*1)-BN-ReLU-AdaptivePool(4)	128*4
	6	Flatten	512
	7	Dense(512)-Dense(256)-Dense(64)-Dense( $n_p$ )	$n_p$

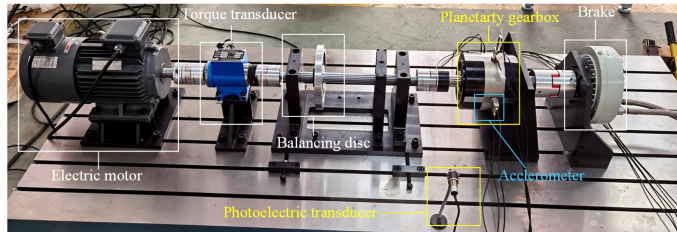


Figure 7: The planetary gearbox system.

under five health conditions listed in Table 3, specifically normal state (N), single-point fault (S), double-point fault (D), three-point fault (T) and compound fault (C). The fault diagnosis of the planetary gearbox can be regarded as a 5-class classification task.

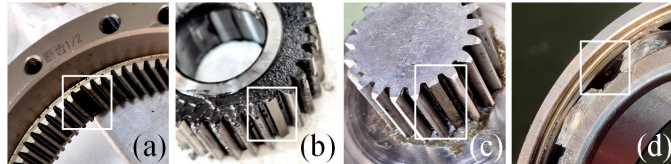


Figure 8: Defective components of the planetary gearbox system. (a) Tooth fracture of the ring gear. (b) Tooth fracture of the sun wheel. (c) Tooth fracture of the planetary gear. (d) Outer race pitting of the rolling bearing.

In data preparation, the raw vibration signal is truncated without overlap through a sliding window to obtain input samples. Each category contains 400 samples, and the length of each sample is set to 1024. After preparation, 60% of the samples are randomly divided as the training set, and the rest samples are used as the test set.

To test the performance of TFconv layer with different kernel functions and different channel numbers, this experiment contains six types of models: the backbone CNN (denoted as CNN), TFN with random kernel (Random-TFN), TFNs with STTF, Chirplet, Morlet Wavelet, and Laplace Wavelet as kernel functions (denoted as STTF-TFN, Chirplet-TFN, Morlet-TFN, Laplace-TFN, respectively). Each type of TFN contains 4 different channel numbers of TFconv layer: 8, 16, 32 and 64. The loss function of classification is cross entropy, the training optimizer is Adam, the momentum is set to 0.9, the initial learning rate is 0.001, the decay rate is 0.96, and the training epoch is 50. To eliminate randomness and verify the stability, each model is repeated 20 times. The results are shown in Fig. 9.

According to Fig. 9, the backbone CNN, as a benchmark, has the worst diagnosis accuracy, and Random-TFN performs slightly better than the backbone CNN does. Morlet-TFN and Laplace-TFN perform better than both CNN and Random-TFN do. STTF-TFN and Chirplet-TFN achieve the best overall diagnosis performance, which demonstrates the effectiveness of proposed method. The effects of the channel number depends on the kernel functions of TFconv layer. Specifically, The channel number has little effect on the performance of STTF-TFN and Chirplet-TFN, because the time-frequency window for these two layers are fixed and sufficient information can be extracted even with limited channels. By contrast, the accuracy of Morlet-TFN and Laplace-TFN decreases significantly with fewer TFconv layer

Table 3: The Working Condition of Gearbox System

Label	Failure Component	Training/Testing sample
N	None	1200/800
S	Ring Gear	1200/800
D	Ring Gear and Sun Wheel	1200/800
T	Ring Gear, Sun Wheel and Planetary Gear	1200/800
C	Ring Gear and Rolling Bearing	1200/800

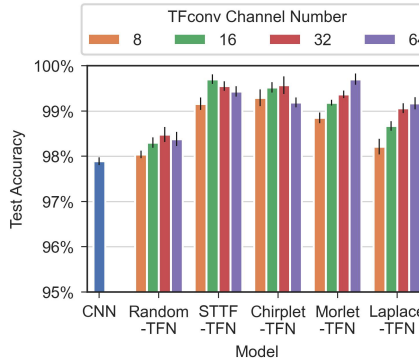


Figure 9: Test accuracy on planetary gearbox dataset.

channels, because the Morlet wavelet and the Laplace wavelet have an adaptive time-frequency window (as illustrated in Fig. 4), and sufficient information can only be extracted with sufficient channels for .

#### 4.2 Aerospace Bearing Dataset

In this subsection, an aerospace bearing dataset is used to verify the diagnosis performance of TFN. The aerospace bearing is the core component of the flywheel test rig, which consists of motor components, a aerospace bearing, a flywheel assembly, the shell, and a mounting base as shown in Fig. 10(a). The flywheel is driven by an electric motor, and then puts the aerospace bearing to work. The data acquisition equipment is shown in Fig. 10(b), including an accelerometer, power supply, a signal acquisition, and analysis system. The flywheel is fixed on an upright bracket, where the acceleration sensor collects the three-way vibration signals of the aerospace bearing at the sampling frequency of 25.6 kHz.

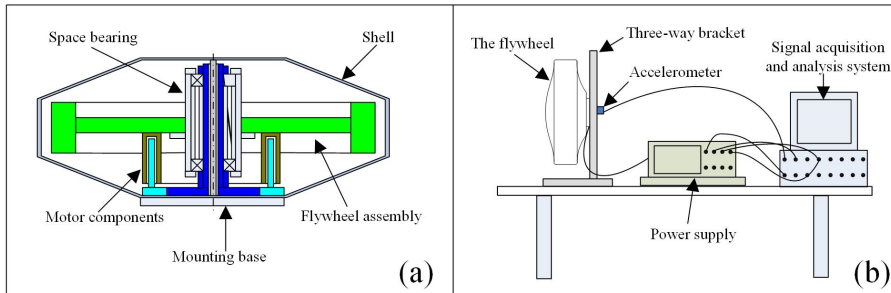


Figure 10: The configuration of aerospace bearing experimental system. (a) Structure of the flywheel. (b) Schematic of the flywheel vibration acquisition process.

The space bearing dataset has five types of health conditions: normal state (N), leading surface scratching (S), cage fault (C), ball fault (B) and inner ring fault (I). For each condition, the radial vibration signal is truncated into samples, and each category contains 1000 samples, for a total of 5000 samples. Then 60% of the samples in each category are used for training, and the remaining samples are used for testing. The fault diagnosis of CWRU rolling bearing can be

regarded as a 5-class classification task. The rest of the setup for this experiment is consistent with that of the previous planetary gearbox experiment.

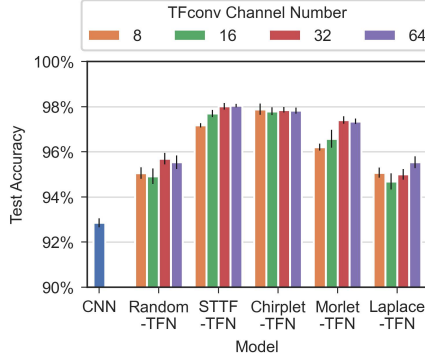


Figure 11: Test accuracy on aerospace bearing dataset.

The experimental results are shown in Fig. 11. The performance of the Backbone CNN is the worst and Random-TFN performs much better. This may be caused by the increased model depth of the newly added convolutional layer, even it is randomly initialized and updated through BP process. As for TFNs, the diagnosis accuracy of Laplace-TFN is close to that of Base-CNN, while STTF-TFN, Chirplet-TFN, and Morlet-TFN have superior performances on diagnosis accuracy, where STTF-TFN with 32 or 64 channels achieves the highest average accuracy of 98.0%. TFconv layer with more channels could extract more time-frequency information and lead to a higher diagnosis accuracy, but it also cost more time in BP process. In conclusion, the kernel function and channel number of TFconv layer are all pivotal to the diagnosis accuracy of the TFN, and proposed TFNs have a much better performance than both backbone CNN and TFN with random kernel.

### 4.3 CWRU Public Bearing Dataset

The CWRU bearing dataset [41] is one of the most popular open source datasets for mechanical fault diagnosis. In order to better spread our work, we choose this open source dataset as a benchmark to test the performance of TFNs and readers can download our code to reproduce this experiment easily. The CWRU bearing experimental system is shown in Fig. 12. The accelerometer is installed on the motor casing of the drive end, and the vibration signals are collected under four loading condition (load 0-3HP) at two sampling frequencies of 12 kHz and 48 kHz.

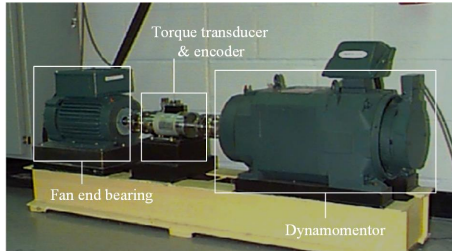


Figure 12: CWRU bearing experimental system.

In addition to normal condition, three different bearing fault types are contained in this dataset: inner raceway fault, rolling element fault, and outer raceway fault. For each fault type, different fault sizes were achieved respectively, i.e. 0.007, 0.014 and 0.021 inches. Therefore, this dataset has nine fault states and a normal state, ten categories in total. The fault diagnosis of CWRU rolling bearing can be regarded as a 10-class classification.

The vibration signal at a sampling frequency of 48 kHz is chosen for the following diagnosis task. The vibration signal is truncated into samples at the length of 1024 and each state has 400 samples, for a total of 4000 samples. 60% samples in each category are used for training, and the remaining samples are used for testing. The rest of the setup for this experiment is consistent with that for the previous planetary gearbox experiment.

The fault diagnosis results of CWRU bearing dataset are shown in Fig. 13. As for diagnosis accuracy, the backbone CNN is always the worst, Random-TFN performs a little better, and Laplace-TFN gets higher accuracy than both the

former two models do, but becomes worse in the 3HP loading condition. STTF-TFN, Chirplet-TFN and Morlet-TFN have excellent performance on fault diagnosis accuracy in all situations. Besides, as the channel number increases, the TFconv layer can extract more time-frequency information, so that the TFN can achieve a higher diagnosis accuracy, but the accuracy of 32 channels and 64 channels are very close. This indicates that 32 channels are enough to extract sufficient fault-related information for diagnosis classification. Except for Laplace-TFN, other TFNs perform much better than backbone CNN and Random-TFN do in all load conditions, which demonstrates the effectiveness of proposed TFNs in fault diagnosis.

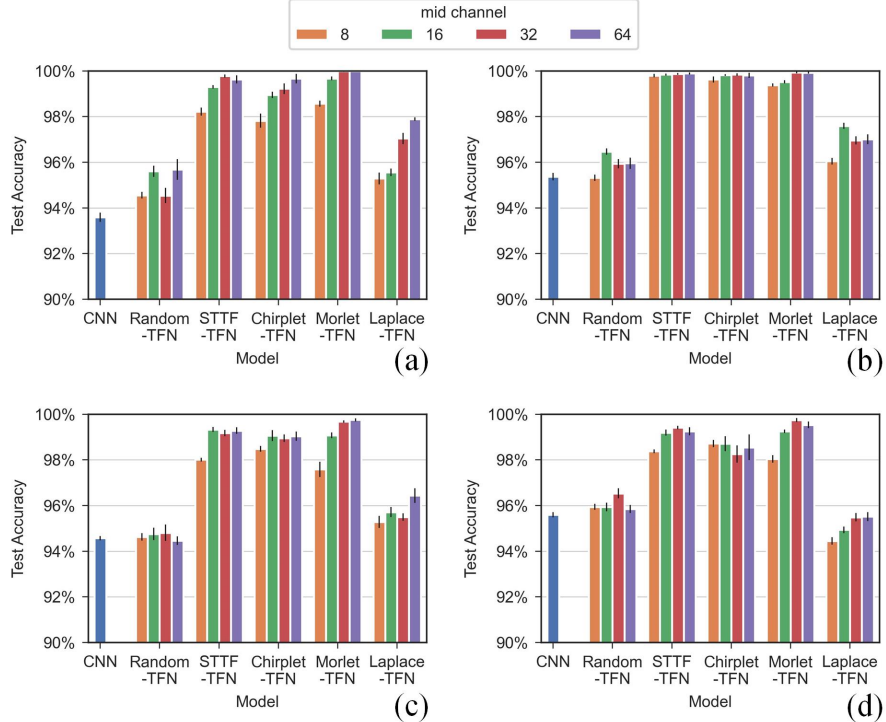


Figure 13: Test accuracy on CWRU bearing dataset with different loading conditions. (a) 0HP. (b) 1HP. (c) 2HP. (d) 3HP.

## 5 Discussion

To further analyze the properties of TFN, ablation experiment, interpretability analysis, visualization analysis, and generalizability analysis are conducted on the CWRU open source dataset. Specifically, the ablation experiment aims to verify the effectiveness of real-imaginary mechanism and the combination between the TFconv layer and the backbone CNN. In interpretability analysis, the interpreting method, proposed in Section III.C, is conducted to explain the focusing frequency area of TFNs in prediction-making. The visualization analysis shows that a better high-dimensional representation could be formulated with the fault-related information extracted by TFconv layer. Finally, the generalizability analysis proves the feasibility of generalizing TFconv layer to other CNN models.

### 5.1 Ablation Study

The main differences between TFNs and traditional CNNs boil down to three aspects: real-imaginary mechanism, kernel function in TFconv layer, and the combination between the TFconv layer and the backbone CNN. As the effectiveness of kernel function has been fully verified in the previous three experiments, the verification of other two aspects is the main purpose here. WaveletKernelNet (WKN) [35], introducing kernel function only to CNN, is used for comparison. In this ablation study, the vibration signal under the 3HP load condition of CWRU bearing dataset is used as input samples, and five types of models are considered for comparison: the backbone CNN, the TFN obtained by adding TFconv layer to the backbone CNN (TFN, the proposed method), the TFN obtained by replacing the first convolutional layer of the backbone CNN with TFconv layer (TFN-replace), the WKN obtained by addition (WKN-add), and the

WKN obtained by replacement (WKN-replace). Moreover, four types of kernel functions are considered in each model: STTF, Chirplet, Morlet wavelet and Laplace wavelet, and the channel number is set to 32.

Table 4: Classification Results of Four Models in Ablation Study

Model	Kernel	Accuracy	Variance
Backbone CNN	-	95.60	0.115
TFN	STTF	<b>99.41</b>	0.073
	Chirplet	<b>98.26</b>	0.380
	Morlet	<b>99.74</b>	0.086
	Laplace	96.02	0.179
TFN-replace	STTF	95.11	0.187
	Chirplet	95.16	0.205
	Morlet	96.73	0.164
	Laplace	93.75	0.132
WKN-add	STTF	97.29	0.213
	Chirplet	96.89	0.232
	Morlet	97.03	0.136
	Laplace	<b>96.43</b>	0.194
WKN-replace	STTF	97.79	0.301
	Chirplet	95.77	0.283
	Morlet	96.64	0.491
	Laplace	95.34	0.103

The results of ablation study are shown in Table 4. The accuracy of Backbone CNN and TFN-replace models are relatively poor, and the accuracy of the WKN-replace models and WKN-add models are significantly improved, while TFN models proposed in this article have the best comprehensive performance. This indicates the effectiveness of the real-imaginary mechanism and the kernel function. The poor performance of TFN-replace could be caused by the conflict between the TFconv layer and the subsequent BN layer in the backbone CNN, where the absolute value produced by TFconv layer is normalized to a target distribution inappropriately and the fault-related information is attenuated. In addition, the performance of different kernel functions are the same as that in previous experiments. The performance of STTF is close to that of Morlet wavelet and achieves the best accuracy overall, and is followed by that of Chirplet. Laplace model has the worst accuracy, similar to Backbone CNN.

## 5.2 Interpretability Analysis

With TFT method embedded into TFconv layer by means of the kernel function, the CNN becomes physically interpretable. Through the interpreting method proposed in Section III, the focusing frequency area of TFN in prediction-making could be revealed.

The vibration signals at 12 KHz sampling frequency under 3HP load condition in the CWRU dataset are used as the input samples, and TFNs with different kernel functions are trained by them. In order to obtain a clear interpretable observation, the channel number of TFNs is set to 8 and other experimental settings are the same as those in the previous experiments.

According to frequency response analysis (Eq.10), the O-FR of the first layer in different models could be obtained. The frequency spectrum of CWRU dataset and the O-FR results are shown in Fig. 14. From the frequency spectrum of CWRU dataset (Fig. 14(a)), it could be observed that the frequency amplitude mainly exists in the four information frequency bands, i.e. band 1-2-3-4, which carry important information for fault diagnosis and have been marked out. These information bands are responsible for fault diagnosis and CNN models should focus on them to obtain a satisfying diagnosis accuracy. From the O-FR results, it could be concluded that

1. The O-FR of trained backbone CNN has an amplitude increase only in the band 4, indicating that the information is insufficiently extracted for fault diagnosis.
2. The O-FR of trained STTF-TFN has amplitude peaks on all the information frequency bands. It means that STTF-TFN pays correct attention to these information bands, which is consistent with its outstanding performance in fault diagnosis. However, since the parameter of STTF kernel function can only change the

centering frequency, not the bandwidth, there still exist some amplitude peaks outside the information bands (i.e. two amplitude peaks in high frequency area).

3. The O-FR of trained Chirplet-TFN has amplitude peaks within all the information frequency bands as well. However, different from STTF-TFN, the Chirplet kernel function has an additional linear frequency modulation factor to change its bandwidth, so there exists no amplitude peak outside the information bands. The O-FR of Chirplet-TFN is completely consistent with the frequency spectrum of CWRU dataset, and Chirplet-TFN achieves the best physical interpretability.
4. The O-FRs of Morlet-TFN and Laplace-TFN change little after training, where three amplitude peaks (corresponding to band 1-3-4) can be barely identified. Although the adaptive frequency bandwidth of wavelet can help to extract fault-related information, it also blurs the focusing frequency bands and thus prevents them from being identified. This leads to the inferior interpretability of Morlet-TFN and Laplace-TFN compared with STTF-TFN and Chirplet-TFN. Due to the asymmetric waveform, the O-FR of Laplace Wavelet kernel function is flatter than that of the Morlet Wavelet kernel function, which makes TFconv layer not be able to concentrate on the information frequency bands and causes the poor diagnosis performance of the Laplace-TFN to some extent.

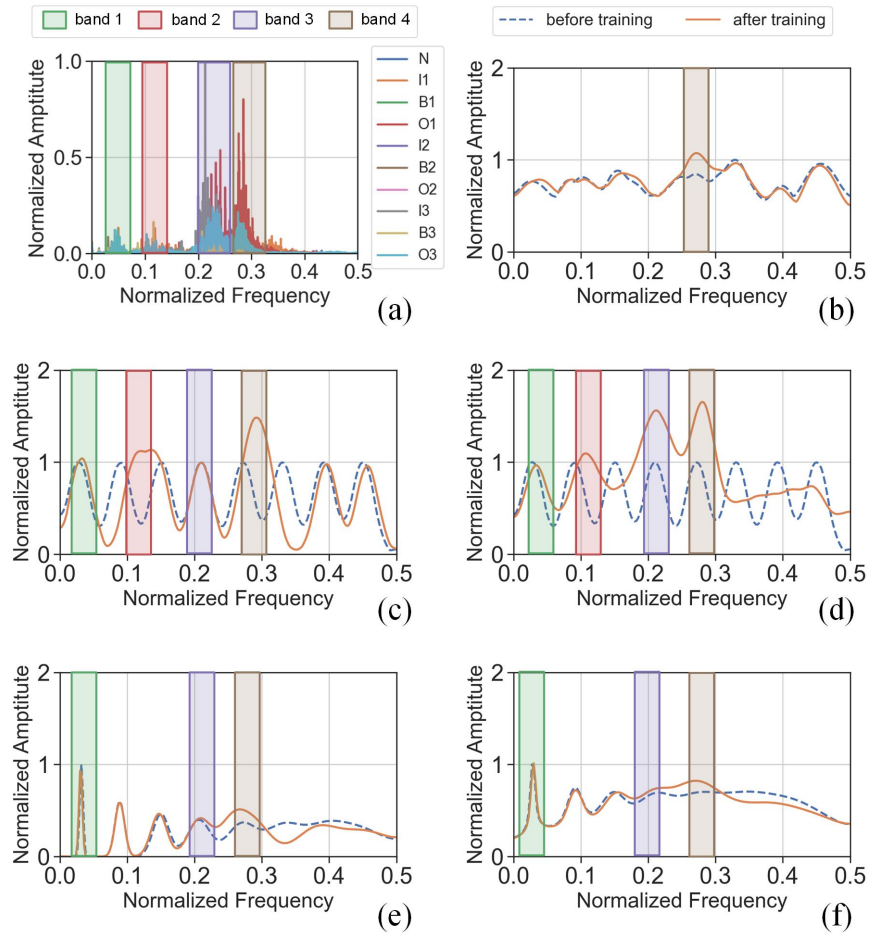


Figure 14: Frequency Spectrum of Dataset and O-FRs of different models. (a) Frequency Spectrum of CWRU Dataset. (b) O-FR of the first layer of backbone CNN. (c) O-FR of the first layer of STTF-TFN. (d) O-FR of the first layer of Chirplet-TFN. (e) O-FR of the first layer of Morlet-TFN. (f) O-FR of the first layer of Laplace-TFN.

### 5.3 Visualization

TFconv layer can not only bring physical interpretability, but also extract fault-related time-frequency information to obtain a better representation. This subsection visualizes the representations of six models discussed above, i.e. the

backbone CNN, Random-TFN, and TFNs with different kernel functions. The results of visualization illustrate the ability of TFconv layer to facilitate representation learning.

The representations are obtained after the process of the convolutional part in CNN models. The vibration signal under 3HP load condition of CWRU dataset is used as the input samples, and the representations of six models are collected and visualized by t-distributed stochastic neighbor embedding (t-SNE) method, as shown in Fig. 15. The representations of Backbone CNN, Random-TFN and Laplace-TFN are so vague to separate their categories. By contrast, STTF-TFN, Chirplet-TFN, and Morlet-TFN have superior representations than the three models mentioned before. Therefore, except for the asymmetric Laplace kernel function, the TFconv layers with other kernel functions can facilitate the CNN model to obtain a better classification representation because of the fault-related time-frequency information extracted by them.

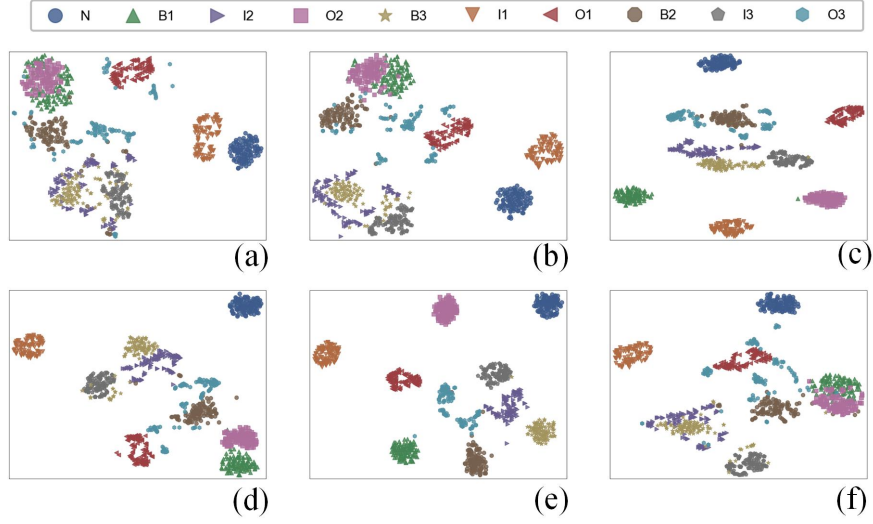


Figure 15: Visualization results of different models. (a) backbone CNN. (b) Random-TFN. (c) STTF-TFN. (d) Chirplet-TFN. (e) Morlet-TFN. (f) Laplace-TFN.

#### 5.4 Generalizability

In order to verify the generalizability of TFconv layer, three typical CNNs with different depths are selected as backbone to obtain different TFNs, whose diagnosis performance is tested in this experiment. The vibration signal under 3HP load condition of CWRU dataset is used as the input samples, and the channel number of TFconv layer is set to 32. Other experimental settings are consistent with those in the previous experiments, and the diagnosis results are shown in Table 5.

It can be seen from the results that, except for the Laplace kernel function, other kernel functions can significantly improve the diagnostic accuracy on the basis of different backbone CNNs. The STTF and Morlet kernels are tied for the highest accuracy, followed by the Chirplet kernel. As for Laplace kernel function, it is slightly better than its backbone CNN, but even worse in terms of the accuracy when the backbone is AlexNet, which may be caused the mismatch between the asymmetric wave and stationary input signals. This experiment shows that the proposed TFconv layer is a general method and it can be applied to other CNNs with different depths to improve their diagnosis performance. Besides, this experiment illustrates the importance of the backbone model. We recommend that users adopt TFconv layer with STTF or Morlet kernel functions, and then combines a backbone CNN with enough depth to formulate the TFN.

## 6 Conclusion

In this article, an interpretable time-frequency convolutional (TFconv) layer is proposed to extract fault-related time-frequency information. Taking TFconv layer as a preprocessing layer, we formulated the Time-Frequency Network (TFN) to achieve higher diagnosis accuracy and explain the focusing frequency area in prediction-making. The effectiveness of TFN has been verified by three sets of mechanical fault diagnosis experiments. The conclusions of this article could be summarized as follows: 1) The participation of TFconv layer can greatly improve the diagnosis

Table 5: Diagnosis Results of Generalizing TFconv Layers to Other CNN Architectures

Backbone	Combined with	Accuracy	Variance
LeNet	None	88.35	0.077
	TFconv-STTF	93.44	0.171
	TFconv-Chirplet	92.76	0.238
	TFconv-Morlet	<b>95.53</b>	0.144
	TFconv-Laplace	91.02	0.130
AlexNet	None	96.33	0.236
	TFconv-STTF	<b>98.89</b>	0.173
	TFconv-Chirplet	98.43	0.239
	TFconv-Morlet	98.58	0.194
	TFconv-Laplace	94.32	0.641
ResNet	None	96.84	0.249
	TFconv-STTF	<b>99.68</b>	0.156
	TFconv-Chirplet	97.59	0.814
	TFconv-Morlet	99.45	0.130
	TFconv-Laplace	97.63	0.249

accuracy of the CNN in mechanical fault diagnosis tasks. 2) The TFconv layer could explain the focusing frequency area of TFN to extract features and make predictions. 3) The kernel function and channel number of TFconv layer have great influence on the diagnosis performance of TFN, and TFconv layer with 32-channel STTF kernel can achieve the overall optimum in accuracy, efficiency and interpretability. 4) The TFconv layer has good generalizability and can be generalized to other CNN models. In future research, we will explore other kernel functions with adaptive frequency bandwidth to interpret focusing frequency more explicitly, and investigate the effectiveness of TFconv layer for other neural networks (e.g. autoencoder).

## Acknowledgments

This project was supported in part by the National Natural Science Foundation of China under Grant 11872243, 12121002 and 51975355; in part by the National Science and Technology Major Project of China under Grant J2019-IV-0018-0086.

## References

- [1] Jimeng Li, Xiangdong Wang, and Hao Wu. Rolling Bearing Fault Detection Based on Improved Piecewise Unsaturated Bistable Stochastic Resonance Method. *IEEE Trans. Instrum. Meas.*, 70:1–9, 2021.
- [2] Yongbo Li, Minqiang Xu, Yu Wei, and Wenhui Huang. An improvement EMD method based on the optimized rational Hermite interpolation approach and its application to gear fault diagnosis. *Measurement*, 63:330–345, 2015.
- [3] Fei Tao, Qinglin Qi, Ang Liu, and Andrew Kusiak. Data-driven smart manufacturing. *J. Manuf. Syst.*, 48:157–169, July 2018.
- [4] Hongtian Chen, Bin Jiang, Steven X. Ding, and Biao Huang. Data-Driven Fault Diagnosis for Traction Systems in High-Speed Trains: A Survey, Challenges, and Perspectives. *IEEE Trans. Intell. Transport. Syst.*, 23(3):1700–1716, March 2022.
- [5] Yaguo Lei, Bin Yang, Xinwei Jiang, Feng Jia, Naipeng Li, and Asoke K. Nandi. Applications of machine learning to machine fault diagnosis: A review and roadmap. *Mech. Syst. Signal Process.*, 138, 2020.
- [6] Ruoyu Li and David He. Rotational Machine Health Monitoring and Fault Detection Using EMD-Based Acoustic Emission Feature Quantification. *IEEE Trans. Instrum. Meas.*, 61(4):990–1001, April 2012.
- [7] Yabin Si, Youqing Wang, and Donghua Zhou. Key-Performance-Indicator-Related Process Monitoring Based on Improved Kernel Partial Least Squares. *IEEE Trans. Ind. Electron.*, 68(3):2626–2636, March 2021.
- [8] Z.K. Peng and F.L. Chu. Application of the wavelet transform in machine condition monitoring and fault diagnostics: A review with bibliography. *Mech. Syst. Signal Process.*, 18(2):199–221, March 2004.

[9] Yongbo Li, Minqiang Xu, Xihui Liang, and Wenhua Huang. Application of Bandwidth EMD and Adaptive Multiscale Morphology Analysis for Incipient Fault Diagnosis of Rolling Bearings. *IEEE Trans. Ind. Electron.*, 64(8):6506–6517, August 2017.

[10] Antonio Brunetti, Domenico Buongiorno, Gianpaolo Francesco Trotta, and Vitoantonio Bevilacqua. Computer vision and deep learning techniques for pedestrian detection and tracking: A survey. *Neurocomputing*, 300:17–33, July 2018.

[11] Haytham M. Fayek, Margaret Lech, and Lawrence Cavedon. Evaluating deep learning architectures for Speech Emotion Recognition. *Neural. Netw.*, 92:60–68, August 2017.

[12] David Silver, Julian Schrittwieser, Karen Simonyan, Ioannis Antonoglou, Aja Huang, Arthur Guez, Thomas Hubert, Lucas Baker, Matthew Lai, Adrian Bolton, Yutian Chen, Timothy Lillicrap, Fan Hui, Laurent Sifre, George van den Driessche, Thore Graepel, and Demis Hassabis. Mastering the game of Go without human knowledge. *Nature*, 550(7676):354–359, October 2017.

[13] Haidong Shao, Hongkai Jiang, Haizhou Zhang, and Tianchen Liang. Electric Locomotive Bearing Fault Diagnosis Using a Novel Convolutional Deep Belief Network. *IEEE Trans. Ind. Electron.*, 65(3):2727–2736, March 2018.

[14] Yu Wang, Ruonan Liu, Di Lin, Dongyue Chen, Ping Li, Qinghua Hu, and C. L. Philip Chen. Coarse-to-Fine: Progressive Knowledge Transfer-Based Multitask Convolutional Neural Network for Intelligent Large-Scale Fault Diagnosis. *IEEE Trans. Neural Netw. Learning Syst.*, 2021.

[15] Xiaoli Zhao, Jianyong Yao, Wenxiang Deng, Peng Ding, Yifei Ding, Minping Jia, and Zheng Liu. Intelligent Fault Diagnosis of Gearbox Under Variable Working Conditions With Adaptive Intraclass and Interclass Convolutional Neural Network. *IEEE Trans. Neural Netw. Learning Syst.*, pages 1–15, 2022.

[16] Dandan Peng, Huan Wang, Zhiliang Liu, Wei Zhang, Ming J. Zuo, and Jian Chen. Multibranch and Multiscale CNN for Fault Diagnosis of Wheelset Bearings Under Strong Noise and Variable Load Condition. *IEEE Trans. Ind. Inf.*, 16(7):4949–4960, July 2020.

[17] Xiaoyin Nie and Gang Xie. A novel normalized recurrent neural network for fault diagnosis with noisy labels. *J. Intell. Manuf.*, 32(5):1271–1288, June 2021.

[18] Z. Zhao, T. Li, J. Wu, C. Sun, S. Wang, R. Yan, and X. Chen. Deep learning algorithms for rotating machinery intelligent diagnosis: An open source benchmark study. *ISA Trans.*, 107:224–255, December 2020.

[19] Quan-shi Zhang and Song-chun Zhu. Visual interpretability for deep learning: A survey. *Front. Inf. Technol. Electron. Eng.*, 19(1):27–39, January 2018.

[20] Peng-Peng Xi, Yong-Ping Zhao, Pei-Xiao Wang, Zhi-Qiang Li, Ying-Ting Pan, and Fang-Quan Song. Least squares support vector machine for class imbalance learning and their applications to fault detection of aircraft engine. *Aerosp. Sci. Technol.*, 84:56–74, January 2019.

[21] Maksims Ivanovs, Roberts Kadikis, and Kaspars Ozols. Perturbation-based methods for explaining deep neural networks: A survey. *Pattern Recognit. Lett.*, 150:228–234, October 2021.

[22] Feng-Lei Fan, Jinjun Xiong, Mengzhou Li, and Ge Wang. On Interpretability of Artificial Neural Networks: A Survey. *IEEE Trans. Radiat. Plasma Med. Sci.*, 5(6):741–760, November 2021.

[23] Yu Zhang, Peter Tino, Ales Leonardis, and Ke Tang. A Survey on Neural Network Interpretability. *IEEE Trans. Emerg. Top. Comput. Intell.*, 5(5):726–742, October 2021.

[24] Amit Dhurandhar, Pin-Yu Chen, Ronny Luss, Chun-Chen Tu, Paishun Ting, Karthikeyan Shanmugam, and Payel Das. Explanations based on the Missing: Towards Contrastive Explanations with Pertinent Negatives. In *Proc. Adv. Neural Inf. Process. Syst. (NeurIPS)*, volume 31. Curran Associates, Inc., 2018.

[25] Yulong Wang, Hang Su, Bo Zhang, and Xiaolin Hu. Interpret Neural Networks by Identifying Critical Data Routing Paths. In *Proc. IEEE Conf. Comput. Vis. Pattern Recog. (CVPR)*, pages 8906–8914, Salt Lake City, UT, June 2018. IEEE.

[26] David Bau, Bolei Zhou, Aditya Khosla, Aude Oliva, and Antonio Torralba. Network Dissection: Quantifying Interpretability of Deep Visual Representations. In *Proc. IEEE Conf. Comput. Vis. Pattern Recog. (CVPR)*, pages 3319–3327, Honolulu, HI, July 2017. IEEE.

[27] Karen Simonyan, Andrea Vedaldi, and Andrew Zisserman. Deep inside convolutional networks: Visualising image classification models and saliency maps. *arxiv:1312.6034.*, 2013.

[28] Ramprasaath R. Selvaraju, Michael Cogswell, Abhishek Das, Ramakrishna Vedantam, Devi Parikh, and Dhruv Batra. Grad-CAM: Visual Explanations from Deep Networks via Gradient-Based Localization. In *Proc. IEEE Int. Conf. Comput. Vis. (ICCV)*, pages 618–626, Venice, October 2017. IEEE.

[29] Mukund Sundararajan, Ankur Taly, and Qiqi Yan. Axiomatic attribution for deep networks. In *Proc. 34th Int. Conf. Mach. Learn. (ICML)*, volume 70, pages 3319–3328. PMLR, August 2017.

[30] Pang Wei Koh and Percy Liang. Understanding black-box predictions via influence functions. In *Proc. 34th Int. Conf. Mach. Learn. (ICML)*, pages 1885–1894, Sydney, NSW, Australia, 2017. JMLR.

[31] Jie Li, Yu Wang, Yanyang Zi, and Zhijie Zhang. Whitening-Net: A Generalized Network to Diagnose the Faults Among Different Machines and Conditions. *IEEE Trans. Neural Netw. Learning Syst.*, pages 1–14, 2021.

[32] Xinya Wu, Yan Zhang, Changming Cheng, and Zhike Peng. A hybrid classification autoencoder for semi-supervised fault diagnosis in rotating machinery. *Mech. Syst. Signal Process.*, 149:107327, February 2021.

[33] Dong Wang, Yikai Chen, Changqing Shen, Jingjing Zhong, Zhike Peng, and Chuan Li. Fully interpretable neural network for locating resonance frequency bands for machine condition monitoring. *Mech. Syst. Signal Process.*, 168:108673, April 2022.

[34] Baoxuan Zhao, Changming Cheng, Guowei Tu, Zhike Peng, Qingbo He, and Guang Meng. An Interpretable Denoising Layer for Neural Networks Based on Reproducing Kernel Hilbert Space and its Application in Machine Fault Diagnosis. *Chin. J. Mech. Eng. (Engl. Ed.)*, 34(1), 2021.

[35] Tianfu Li, Zhibin Zhao, Chuang Sun, Li Cheng, Xuefeng Chen, Ruqiang Yan, and Robert X. Gao. WaveletKernel-Net: An Interpretable Deep Neural Network for Industrial Intelligent Diagnosis. *IEEE Trans. Syst. Man Cybern. Syst.*, 52(4):2302–2312, April 2022.

[36] Yang Yang, Wenming Zhang, Zhike Peng, and Guang Meng. Multicomponent Signal Analysis Based on Polynomial Chirplet Transform. *IEEE Trans. Ind. Electron.*, 60(9):3948–3956, September 2013.

[37] Michael X Cohen. A better way to define and describe Morlet wavelets for time-frequency analysis. *NeuroImage*, 199:81–86, October 2019.

[38] Tariq Abuhamdia, Saeid Taheri, and John Burns. Laplace wavelet transform theory and applications. *J. Vib. Control.*, 24(9):1600–1620, May 2018.

[39] Vincent Andrearczyk and Paul F Whelan. Using filter banks in convolutional neural networks for texture classification. *Pattern Recognit. Lett.*, 84:63–69, 2016.

[40] Alan V Oppenheim, Alan S Willsky, Syed Hamid Nawab, Gloria Mata Hernández, et al. *Signals & Systems*. Pearson Educación, 1997.

[41] Wade A. Smith and Robert B. Randall. Rolling element bearing diagnostics using the Case Western Reserve University data: A benchmark study. *Mech. Syst. Signal Process.*, 64–65:100–131, December 2015.